Full-Wave Analysis of MICs in Multilayer Dielectric Media in a Rectangular Waveguide

Odilon M. C. Pereira Filho, *Member, IEEE*, and Tapan K. Sarkar, *Fellow, IEEE*

***Abstract*—A full-wave analysis of microwave integrated circuits in multilayer dielectric media in a rectangular waveguide is described. It combines spectral-domain approach with residue theory and the contour integration method to accurately evaluate the impedance matrix of the method of moments. The S-parameters are obtained by exciting the circuit with a voltage gap generator and applying the matrix pencil technique, or by impressing traveling-wave currents. Modifications on the latter are introduced. Both methods are compared from a physical point-of-view, analytical complexity, and numerical efficiency.**

***Index Terms*—Full wave, matrix pencil, MIC, multilayered structure, waveguide.**

I. Introduction

A LARGE number of techniques have been applied to microwave integrated circuits (MICs), from quasi-static analysis to full-wave procedures. A good overview of these methods used to characterize frequency-dependent microstrip components and discontinuities is given in [1]. Originally these circuits were build over one dielectric layer [2], but recently, additional layers have been included for improving the performance of the devices or to reduce the complexity of the circuits [3]–[9]. Furthermore, they provide alternate solutions to circuit layout, new feeding structures, and even mechanical protection as superstrates.

Although very accurate, application of full-wave techniques using the method of moments (MoM) are often time consuming. In space domain, this results from the multiple integrations (in the testing region, source region, and from the representation of the Green's functions) to be performed for obtaining the elements of the impedance matrix of the MoM. In the spectral-domain approach, it is a consequence of the oscillatory behavior of the transforms of the source and testing functions, together with the slow decaying transform of the Green's functions. Recently, an effort has been made to overcome these difficulties, allowing for such an analysis to be quickly performed on computer-aided design (CAD) packages. For the open case in space domain, the elements are often calculated by interpolation of previously obtained Sommerfeld integrals [10]. Alternatively, the quasi-static term and the surface waves can be extracted from the original form of the element, and the remaining portion of the Green's function is expanded in a series of exponentials [11]. In the spectral domain, for the same open case, the impedance matrix involves evaluation of doubly infinite integrations. It has been proposed in [12] and [13] that the inner integration be numerically evaluated only up to a point where the Green's functions approach its asymptotic form, which contains only algebraic functions. The remaining portion of the integral can be either evaluated in closed form or deformed to an integral with an exponentially decaying integrand. For the case of boxed MICs, the impedance matrix can be efficiently evaluated through fast Fourier transform (FFT) algorithms [14]–[16]. The technique can be applied only to the cases in which the surface of the circuit can be discretized into an uniform mesh. Even when it is possible, the maximum segment length of the mesh, in each direction, is the greatest common denominator of the circuit dimensions. In general, it may represent an unnecessarily large number of basis functions. In [17], residue theory and the contour integral method are used to transform one of the double infinite summations into an integral around the branch cut. This integral is lately replaced by a summation of two consecutive integrations of the modified Bessel function of zeroth-order K_o. Very recently [18], Poison's summation formula together with Sommerfeld's identity was used to convert one of the summations in the Green's functions into a summation of modified Bessel functions K_o and K_1.

In this paper, we present a full-wave analysis of a planar MIC in a multilayer dielectric media in a rectangular waveguide. It used the spectral-domain approach, and the elements of the moment matrix are evaluated by subtracting a conveniently modified asymptotic limit of its integrand. The integral of the limit is obtained using residue theory and the contour integration method, resulting in a faster and more accurate procedure. We also study and compare two excitation techniques often used in the literature, i.e., the voltage gap generator, and the traveling-wave impressed current [5], [13], [19]. Some modifications are introduced in the latter for both the basis and weighting functions, which ensure the stability of the results. Our aim is to evaluate the mathematical models from both the practical point-of-view and numerical efficiency. The analysis will be performed for a two-port network, although it can be easily extended to an arbitrary number of ports.

II. Green's Functions and MoM

Consider a rectangular waveguide, whose cross section is shown in Fig. 1. It has dimension a in the x-direction and is filled with three layers of dielectric thickness h_1, h_2, and h_3. Each layer consists of a homogeneous, isotropic, and lossless dielectric characterized by its permittivity (ϵ_i) and permeability

Manuscript received April 8, 1998.

O. M. C. Pereira Filho was with the Department of Electrical Engineering and Computer Science, Syracuse University, Syracuse, NY 13210 USA. He is now with the IBM Corporation, Hopewell Junction, NY 12533 USA.

T. K. Sarkar is with the Department of Electrical Engineering and Computer Science, Syracuse University, Syracuse, NY 13210 USA.

Publisher Item Identifier S 0018-9480(00)08722-6.

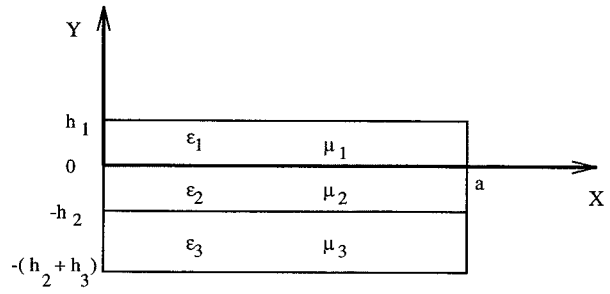

Fig. 1. Cross section of the waveguide.

(μ_i). All metals are assumed to be perfect conductors, and a time variation of e^{jwt} is assumed and suppressed.

Suppose that an arbitrary surface current distribution exists at the dielectric interfaces. The electromagnetic fields in each layer can be expressed in terms of any two components of the vector potentials. In the spectral-domain approach, it is common to choose the components of the vector potentials in the direction normal to the dielectric interfaces (A_y, F_y), as the TM^y and the TE^y components of the fields are decoupled [1], [4]. Furthermore, using the equivalent transmission-line model, additional dielectric layers can be added without any major increase in the complexity of the analysis [4]. From the boundary conditions at $x = 0$ and $x = a$, we observe that $A_{yi}(F_{yi})$, $i = 1, 2$, or 3 can be represented by a sine (cosine) Fourier series in the x-direction and by exponentials in the z-direction. The Green's functions for the vector potentials are obtained by imposing the boundary conditions at the dielectric interfaces, when an electric dipole is present at one of them. Since we need to calculate the electric field only in medium 2 for imposing the boundary condition at the circuits, the Green's functions will be shown only for this layer. Specifically, the partial derivative of the Green's function for the magnetic vector potential in respect to y is shown instead of the function itself, as E_x and E_z depend directly on this derivative.

For an x-directed electric dipole at $y = 0$, $J_s = \hat{a}_x\delta(x - x')\delta(z - z')$, the Green's functions for medium 2, obtained as described before, are given by

$$\frac{\partial \tilde{G}^s{}_{Ax0}}{\partial y} = \frac{\partial \tilde{G}^s{}_{A0x0}}{\partial y}\,\frac{\varepsilon_n}{a}\,\cos(\alpha_n x')\,e^{jk_z z'} \tag{1}$$

$$\tilde{G}^c{}_{Fx0} = \tilde{G}^c{}_{F0x0}\,\frac{\varepsilon_n}{a}\,\cos(\alpha_n x')\,e^{jk_z z'} \tag{2}$$

where

$$\frac{\partial \tilde{G}^s_{A0x0}}{\partial y} = \frac{1}{DTM}\,\frac{\alpha_n k_{y1}(1-\Gamma_{A1})}{\alpha_n^2 + k_z^2} \cdot\left[-\frac{\epsilon_3}{\epsilon_1}\,k_{y2}(1+\Gamma_{A3})\,\frac{\sin(k_{y2}(y+h_2))}{\cos(k_{y2}h_2)} + j\,\frac{\epsilon_2}{\epsilon_1}\,k_{y3}(1-\Gamma_{A3})\,\frac{\cos(k_{y2}(y+h_2))}{\cos(k_{y2}h_2)}\right] \tag{3}$$

$$\tilde{G}^c_{F0x0} = \frac{1}{DTE}\,\frac{k_z w\mu_2}{\alpha_n^2 + k_z^2}\,\frac{(1+\Gamma_{F1})}{k_{y1}} \cdot\left[\frac{j\mu_3}{\mu_2}\,\frac{(1+\Gamma_{F3})}{k_{y3}}\,\frac{\cos(k_{y2}(y+h_2))}{\cos(k_{y2}h_2)} - (1-\Gamma_{F3})\frac{\sin(k_{y2}(y+h_2))}{k_{y2}\cos(k_{y2}h_2)}\right] \tag{4}$$

$$\begin{aligned} DTM = &-\frac{\epsilon_3}{\epsilon_1}\,k_{y1}(1-\Gamma_{A1})(1+\Gamma_{A3}) \\ &- j\frac{\epsilon_2}{\epsilon_1}\,\frac{k_{y1}k_{y3}}{k_{y2}}(1-\Gamma_{A1})(1-\Gamma_{A3})\tan(k_{y2}h_2) \\ &\cdot\tan(k_{y2}h_2) - k_{y3}(1+\Gamma_{A1})(1-\Gamma_{A3}) \end{aligned} \tag{5}$$

$$\begin{aligned} DTE = &-\frac{\mu_3}{\mu_1}(1-\Gamma_{F1})\frac{(1+\Gamma_{F3})}{k_{y3}} \\ &- j\frac{\mu_2}{\mu_1}(1-\Gamma_{F1})(1-\Gamma_{F3})\frac{\tan(k_{y2}h_2)}{k_{y2}} \\ &- j\frac{\mu_3}{\mu_2}\,k_{y2}\frac{(1+\Gamma_{F1})(1+\Gamma_{F3})}{k_{y1}k_{y3}}\,\tan(k_{y2}h_2) \\ &- \frac{(1+\Gamma_{F1})}{k_{y1}}(1-\Gamma_{F3}). \end{aligned} \tag{6}$$

When there are only three dielectric layers, the coefficients Γ_A and Γ_F represent the reflection coefficients due to the conductors at $y = h_1$ and $y = -(h_2 + h_3)$. For a larger number of layers, these coefficients represent the reflection coefficients of decoupled TM^y and TE^y modes, obtained through the equivalent transmission-line method [1], [4]. The indexes in $\tilde{G}^s_{Ax0}$ stand for sine transform of the Green's function for A_y due to an x-directed dipole in the $y = 0$ interface. Similarly, for $\tilde{G}^c_{Fx0}$. $DTM = 0$ ($DTE = 0$) is the transcendental equation for the TM^y (TE^y) modes that propagate in the structure without any circuit in the dielectric interfaces. The total vector potential at medium 2 due to some arbitrary x-directed source distribution at $y = 0$, and their transforms, are obtained by superposition.

For the case of a z-directed electric dipole at $y = 0$, $J_s = \hat{a}_z\delta(x - x')\delta(z - z')$, the Green's functions for medium 2 are given by

$$\frac{\partial \tilde{G}^s_{Az0}}{\partial y} = \frac{\partial \tilde{G}^s_{A0z0}}{\partial y}\,\frac{2}{a}\,\sin(\alpha_n x')e^{jk_z z'} \tag{7}$$

$$\tilde{G}^c_{Fz0} = \tilde{G}^c_{F0z0}\frac{2}{a}\,\sin(\alpha_n x')e^{jk_z z'} \tag{8}$$

where

$$\frac{\partial \tilde{G}^s_{A0z0}}{\partial y} = \frac{1}{DTM}\,\frac{jk_z k_{y1}(1-\Gamma_{A1})}{\alpha_n^2 + k_z^2} \cdot\left[-\frac{\epsilon_3}{\epsilon_1}\,k_{y2}(1+\Gamma_{A3})\frac{\sin(k_{y2}(y+h_2))}{\cos(k_{y2}h_2)} + j\frac{\epsilon_2}{\epsilon_1}\,k_{y3}(1-\Gamma_{A3})\frac{\cos(k_{y2}(y+h_2))}{\cos(k_{y2}h_2)}\right] \tag{9}$$

$$\tilde{G}^c_{F0z0} = \frac{1}{DTE}\,\frac{jw\mu_2\alpha_n}{\alpha_n^2 + k_z^2}\,\frac{(1+\Gamma_{F1})}{k_{y1}} \cdot\left[\frac{j\mu_3}{\mu_2}\,\frac{(1+\Gamma_{F3})}{k_{y3}}\,\frac{\cos(k_{y2}(y+h_2))}{\cos(k_{y2}h_2)} - (1-\Gamma_{F3})\frac{\sin(k_{y2}(y+h_2))}{k_{y2}\cos(k_{y2}h_2)}\right]. \tag{10}$$

Similar Green's functions are obtained for the sources at $y = -h_2$, and are omitted here for the sake of space. The integral equation of the problem arises from the boundary conditions on the surface of the circuit (S), supposing the presence of either an incident field $E^{\mathbf{in}}$, or an impressed current. Expanding the current in a set of basis functions (J_{xm_s}, $m_s = 1, \ldots, M_x$; J_{zm_s}, $m_s = 1, \ldots, M_z$) and taking the inner product with weighting functions (W_{xm_f}; $m_f = 1, \ldots, M_x$, W_{zm_f}, $m_f =$

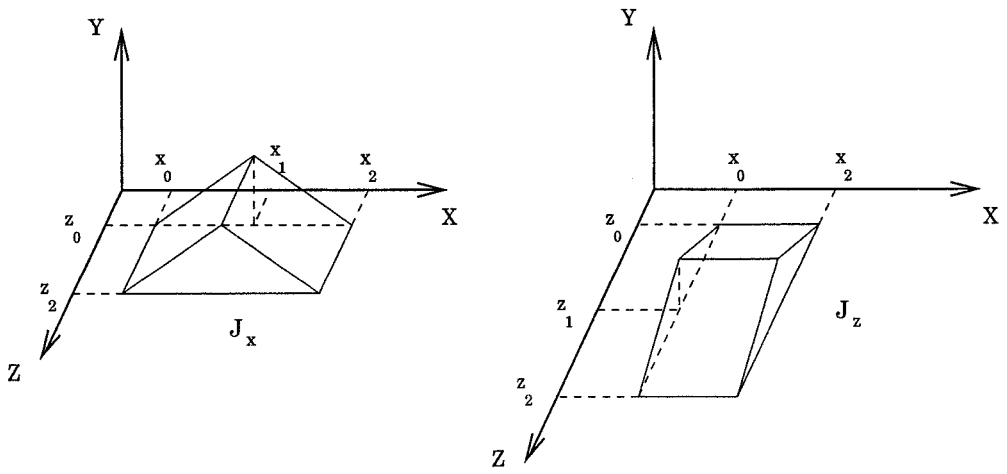

Fig. 2. Rooftop basis functions.

$1, \ldots, M_z$) the integral equation is transformed into a matrix equation given by

$$[Z][I] = [V]. \tag{11}$$

The elements of the vector $[I]$ are the coefficients of the current expansion in the set of basis functions. The vector $[V]$ will depend on the excitation used, and the elements of the impedance matrix $[Z]$ are given by the reaction of the fields due to a basis function J_{m_s}, on a weighting function W_{m_f}.

$$Z_{m_f m_s} = \langle W_{m_f}, E(J_{m_s})\rangle. \tag{12}$$

For example, for the case of a z-directed basis and weighting functions

$$Z_{zzm_f m_s} = \frac{a}{4\pi}\sum_{n=1}^{\infty}\int_{-\infty}^{\infty}\left(\frac{-k_z}{w\epsilon_2}\frac{\partial\tilde{G}^s_{A0z}}{\partial y} + \alpha_n\tilde{G}^c_{F0z}\right) \cdot\tilde{J}^s_{zm_s}(\alpha_n, k_z)\tilde{W}^{s*}_{zm_f}(\alpha_n, k_z)\,dk_z \tag{13}$$

where $\tilde{J}^s_{zm_s}$ and $\tilde{W}^s_{zm_f}$ are the sine transform of the basis and weighting functions.

III. Voltage Gap Generator

The voltage gap generator assumes that an incident electromagnetic field has a delta-function distribution over a dielectric interface [$E^{\text{in}} = \delta(z - z_e)\hat{a}_z$ at $y = 0$ or $y = -h_2$]. The elements of the excitation vector $[V]$ are given by $V_{m_f} = -\langle W_{m_f}, E^{\text{in}}\rangle$. Rooftop functions (Fig. 2) are used as basis functions due to their simplicity and flexibility in approximating the currents on a circuit of arbitrary shape. The same set of functions are used as testing functions, resulting in a Galerkin procedure, and in the symmetry of matrix $[Z]$. The position of the excitation (z_e) is often chosen such that it coincides with the edge of the discretization of the circuit that is closest to the truncation of the input/output lines. As a consequence, the only nonzero testing functions at the excitation point are those centered in z_e. The elements of the matrix $[V]$ are simply given by

$$V_{xm} = 0 \tag{14}$$

$$V_{zm} = \begin{cases} -\Delta x, & \text{if } W_{zm}(x, z_e) = 1 \\ 0, & \text{otherwise} \end{cases} \tag{15}$$

where Δx is the transversal discretization length of the z-directed currents.

A. Numerical Evaluation of the Impedance Matrix Z

In both the space or spectral domains, the elements of the impedance matrix $[Z]$ exhibit slow convergence. In this paper, residue theory and the contour integral method are used, together with some modifications of the asymptotic limit of the integrand that result in a much simpler analysis. The procedure will be illustrated for the Z_{zz} elements, with source at the $y = 0$ interface. From the parity of the integrand, we can write

$$Z_{zzm_f m_s} = \frac{1}{4\pi}\sum_{n=1}^{\infty}\int_0^{\infty}\text{Int}^+_{zz}\,dk_z \tag{16}$$

where

$$\text{Int}^+_{zz} = \left(\frac{-k_z}{w\epsilon_2}\frac{\partial\tilde{G}^s_{A0z0}}{\partial y} + \alpha_n\tilde{G}^c_{F0z0}\right) \cdot\Big[\tilde{J}^s_{zm_s}(\alpha_n, k_z)\tilde{W}^s_{zm_f}(\alpha_n, -k_z) + \tilde{J}^s_{zm_s}(\alpha_n, -k_z)\tilde{W}^s_{zm_f}(\alpha_n, k_z)\Big]. \tag{17}$$

The first numerical problem arises from the poles of the integrand, i.e., the real zeros of DTM and DTE that correspond to the propagation constant k_z of the TM^y and TE^y modes of the rectangular waveguide above cutoff. The numerical problem is overcome by subtracting the singularities from the integrand and analytically evaluating the remaining singular integrals. For waveguides with $a > b = (h_1 + h_2 + h_3)$, the dominant waveguide mode is often the first TM^y mode with $n = 1$, and the pole (k_{z0}) is the first zero of DTM, with $n = 1$. The term corresponding to $n = 1$ is written as

$$Z_{zzm_f m_s|n=1} = \frac{a}{4\pi}\left[\int_0^{k_{z1}} + \int_{k_{z2}}^{\infty}\right]\text{Int}^+_{zz}\,dk_z + \frac{a}{4\pi}\int_{k_{z1}}^{k_{z2}}\left[\text{Int}^+_{zz} - \frac{R'}{k_z - k_{z0}}\right]dk_z + \frac{a}{4\pi}R'\left(\ln\frac{k_{z2} - k_{z0}}{k_{z0} - k_{z1}} - j\pi\right) \tag{18}$$

where $k_{z1} < k_{z0} < k_{z2}$ and $R' = \text{residue of } \text{Int}^+_{zz} \text{ at } k_{z0}$.

The second and more troublesome problem when evaluating the elements of matrix $[Z]$ is due to the slow convergence of the summation and integrals, especially for the case when source and testing functions are in the same interface. The evaluation of the impedance matrix becomes computationally expensive, and its accuracy is endangered by the oscillatory nature of the integrands. To overcome this limitation, the limit of the integrand, as $\sqrt{k_z^2+\alpha_n^2}$ goes to infinity, is added and subtracted to the original integrand

$$Z_{zzm_fm_s} = \frac{a}{4\pi}\sum_{n=1}^{\infty}\left[\int_0^{\infty}\left(\mathrm{Int}_{zz}^{+} - \lim_{\sqrt{k_z^2+\alpha_n^2}\to\infty}\mathrm{Int}_{zz}^{+}\right)\cdot dk_z + L_{zzm_fm_s}\right] \tag{19}$$

where

$$L_{zzm_fm_s} = \int_{-\infty}^{\infty}\lim_{\sqrt{k_z^2+\alpha_n^2}\to\infty}\mathrm{Int}_{zz}\,dk_z \tag{20}$$

and Int_{zz} is the integrand of $Z_{zzm_fm_s}$ in (13), whose asymptotic limit is given by

$$\begin{aligned}&\lim_{\sqrt{k_z^2+\alpha_n^2}\to\infty}\mathrm{Int}_{zz}\\ &=\left(-\frac{C_{2\epsilon}}{jw\epsilon_2C_{1\epsilon}} - jw\mu_2\frac{C_{2\mu}}{C_{1\mu}}\frac{\alpha_n^2}{(k_z^2+\alpha_n^2)k_z^2}\right)\\ &\cdot\frac{F_{zm_s}^s(\alpha_n)F_{zm_f}^s(\alpha_n)}{\sqrt{k_z^2+\alpha_n^2}k_z^2}\\ &\cdot\left[\frac{e^{jk_zz_{1m_s}}-e^{jk_zz_{0m_s}}}{z_{1m_s}-z_{0m_s}}+\frac{e^{jk_zz_{1m_s}}-e^{jk_zz_{2m_s}}}{z_{2m_s}-z_{1m_s}}\right]\\ &\cdot\left[\frac{e^{-jk_zz_{1m_f}}-e^{-jk_zz_{0m_f}}}{z_{1m_f}-z_{0m_f}}+\frac{e^{-jk_zz_{1m_f}}-e^{-jk_zz_{2m_f}}}{z_{2m_f}-z_{1m_f}}\right]\end{aligned} \tag{21}$$

where $C_{i\epsilon}$ and $C_{i\mu}$ are constants that depend on the permittivities and permeabilities of the three layers.

Now, the integral in $Z_{xxm_fm_s}$ (19) can be evaluated quickly as the integrand converges asymptotically to zero. The convergence problems of Z_{zz} have been isolated in $L_{xxm_fm_s}$, which will be evaluated analytically. A basic procedure for evaluating integrals on the real axis is to close the contour with a semicircle of infinite radius (C_∞) and to use the residue theorem. In our case, the limit above has two branch cuts, with branch points at $k_z=\pm j\alpha_n$, a second-order pole at $k_z=0$, and first-order poles at $k_z=\pm j\alpha_n$, as shown in Fig. 3. When applying the contour integral method, it would be necessary to add a path around the branch cut, as in [17], and to deal with a second-order pole in the integration path. Geometrically, the limiting case represents a multilayer media with the layers 1 and 3 extending to $y=\infty$ and $-\infty$, respectively. Those branch cuts account for the corresponding radiation in this now open structure. However, physically they have no meaning to the original problem. We have

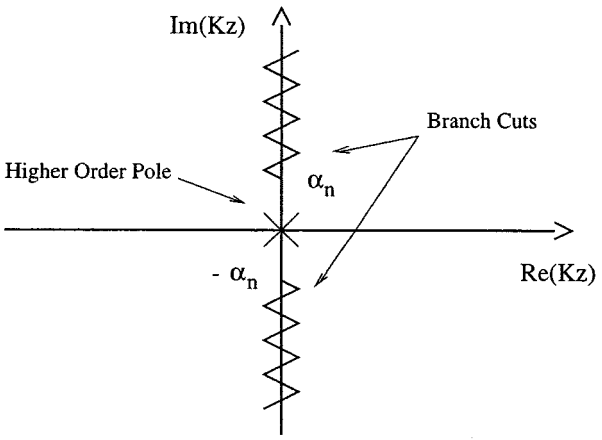

Fig. 3. Singularities of the asymptotic limit in the k_z-plane.

analyzed different ways of expressing this limit that simplifies the analytical evaluation of $L_{xxm_fm_s}$, avoiding the above problems. We are suggesting the following substitutions:

$$\frac{1}{\sqrt{k_z^2+\alpha_n^2}} \to \frac{\tanh\left(\sqrt{k_z^2+\alpha_n^2}\right)}{\sqrt{k_z^2+\alpha_n^2}} \tag{22}$$

$$\frac{1}{k_z^2} \to \frac{1}{k_z^2+(r\pi/a)^2}, \qquad r<1. \tag{23}$$

When applying the contour integral method and residue theory, the integration around the branch cut is substituted by a summation of residues, and the second-order pole at $k_z=0$ is substituted by the first-order poles at $k_z=\pm jr\pi/a$. The singularities of the modified asymptotic limit are shown in Fig. 4. It should be stressed that these modifications do not alter the limit, as the hyperbolic tangent converges rapidly to 1 and $r<1$. After these changes, the limit of the integrand is given by

$$\begin{aligned}&\lim_{\sqrt{k_z^2+\alpha_n^2}\to\infty}\mathrm{Int}_{zz}\\ &=\left(-\frac{C_{2\epsilon}}{jw\epsilon_2C_{1\epsilon}} - jw\mu_2\frac{C_{2\mu}}{C_{1\mu}}\frac{\alpha_n^2}{(k_z^2+\alpha_n^2)[k_z^2+(r_1\pi/a)^2]}\right)\\ &\cdot\frac{\tanh\left(\sqrt{k_z^2+\alpha_n^2}\right)}{\sqrt{k_z^2+\alpha_n^2}[k_z^2+(r_2\pi/a)^2]}\\ &\cdot\left[\frac{e^{jk_zz_{1m_s}}-e^{jk_zz_{0m_s}}}{z_{1m_s}-z_{0m_s}}+\frac{e^{jk_zz_{1m_s}}-e^{jk_zz_{2m_s}}}{z_{2m_s}-z_{1m_s}}\right]\\ &\cdot F_{zm_s}^s(\alpha_n)F_{zm_f}^s(\alpha_n)\\ &\cdot\left[\frac{e^{-jk_zz_{1m_f}}-e^{-jk_zz_{0m_f}}}{z_{1m_f}-z_{0m_f}}+\frac{e^{-jk_zz_{1m_f}}-e^{-jk_zz_{2m_f}}}{z_{2m_f}-z_{1m_f}}\right].\end{aligned} \tag{24}$$

$L_{zzm_fm_s}$ is obtained by substituting (24) into (20), and is written as a combination of the functions f_1 and f_2, given below,

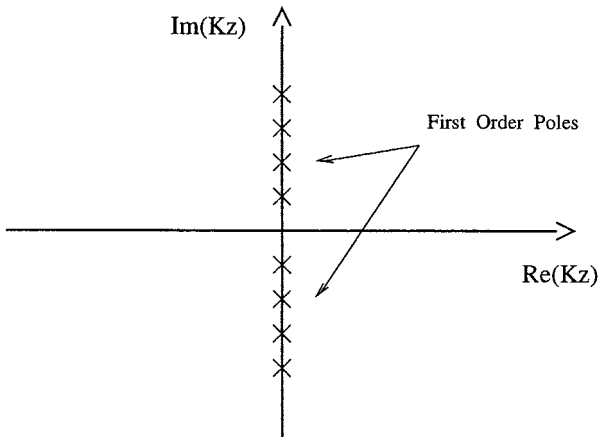

Fig. 4. Singularities of the modified asymptotic limit in the k_z-plane.

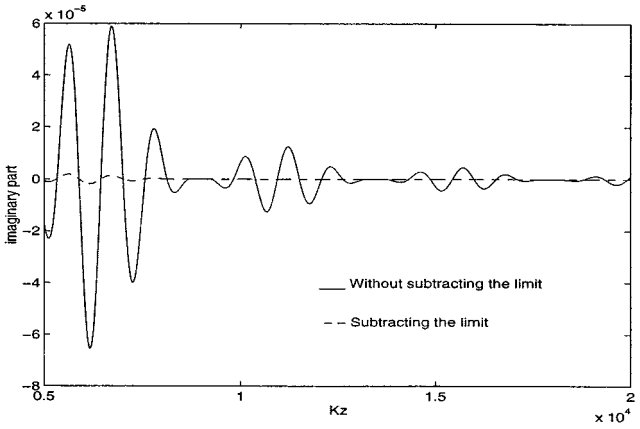

Fig. 5. Original integrand of Zmn and the resulting integrand after subtracting the limit.

which are evaluated using contour integration and the residue theorem

$$f_1(d,r) = \int_{-\infty}^{\infty} e^{j\,dk_z} \frac{\tanh\left(\sqrt{k_z^2+\alpha_n^2}\right)}{(k_z^2+(r\pi/a)^2)\sqrt{k_z^2+\alpha_n^2}}\,dk_z \tag{25}$$

$$= \frac{a^2 e^{-|d|r\pi/a}\tanh\left(\frac{\pi}{a}\sqrt{n^2-r^2}\right)}{r\pi\sqrt{n^2-r^2}} + \sum_{p=1}^{\infty} \frac{2\pi e^{-|d|k_{zp}}}{k_{zp}[(r\pi/a)^2-k_{zp}^2]} \tag{26}$$

$$f_2(d,r_1,r_2) = \int_{-\infty}^{\infty} e^{j\,dk_z} \cdot \frac{\tanh\left(\sqrt{k_z^2+\alpha_n^2}\right)}{(k_z^2+\alpha_n^2)^{3/2}[k_z^2+(r_1\pi/a)^2][k_z^2+(r_2\pi/a)^2]}\,dk_z$$

$$= \frac{\pi e^{-|d|\alpha_n}}{\alpha_n[(r_1\pi/a)^2-\alpha_n^2][(r_2\pi/a)^2-\alpha_n^2]} + \frac{a^6 e^{-|d|r_1\pi/a}\tanh\left(\frac{\pi}{a}\sqrt{n^2-r_1^2}\right)}{r_1\pi^5(n^2-r_1^2)^{3/2}(r_2^2-r_1^2)} + \frac{a^6 e^{-|d|r_2\pi/a}\tanh\left(\frac{\pi}{a}\sqrt{n^2-r_2^2}\right)}{r_2\pi^5(n^2-r_2^2)^{3/2}(r_1^2-r_2^2)} + \sum_{p=1}^{\infty} \frac{2\pi e^{-|d|k_{zp}}}{k_{zp}[(r_1\pi/a)^2-k_{zp}^2][(r_2\pi/a)^2-k_{zp}^2](\alpha_n^2-k_{zp}^2)} \tag{27}$$

where

$$k_{zp} = \sqrt{\left(\frac{(2p-1)\pi}{2}\right)^2+\alpha_n^2}, \qquad p = 1, 2, 3, \ldots. \tag{28}$$

We should observe that the functions f_1 and f_2 are given by exponentially decaying summations, unless $d = 0$. In this case, the summations need to be evaluated only once, and their results stored for future reference. As a result, the integral of the asymptotic limit ($L_{zzm_f m_s}$), where the oscillatory and slow decaying behavior of the integrand has been isolated, is now expressed by an exponentially converging summation, which can be quickly and accurately evaluated. A very similar procedure is used for the elements of the submatrices Z_{xx} and Z_{zx}, where the substitutions (22) and (23) are used, and integrals like f_1 and f_2 are defined and evaluated analytically.

An example of how the procedure described improves the numerical evaluation of the elements of matrix $[Z]$ is shown in Fig. 5. It compares the original integrand of an element of the impedance matrix and the resulting integrand after subtracting the limit. For relatively small values of k_z, the original integrand has already approached the limit, while the first still oscillates. The advantage of the procedure described is to limit the amount of numerical integration performed by drastically improving the behavior of the integrand. Furthermore, the limit of the integrand is reached when $\sqrt{\alpha_n^2+k_z^2}$ goes to ∞. This means that as n increases in evaluation of the elements of $[Z]$, the integrand converge to the asymptotic limit for a smaller value of k_z. As a result, the numerical integration is performed over a decreasing interval length in k_z as n increases. The overall effect is a combination of an increase in the accuracy of the elements of the impedance matrix, and substantial savings in computational time spent to fill out the matrix $[Z]$.

B. Extraction of the S-Parameters

Once the matrices $[Z]$ and $[V]$ are known, the linear system (11) is solved for the currents excited in the circuit. The S-parameters can be obtained from the current distribution, either from the network admittance matrix [20], application of ideal transmission-line theory [9], [21], or using the matrix pencil technique [22], [23]. The latter has been used as it presents two advantages over the previous ones. For reciprocal networks, it does not require the evaluation of the characteristic impedances of the transmission lines in any of the ports of the circuit. Also, it can be applied over a relatively small section of the circuit, which means that a smaller number of basis functions and substantial savings in time to fill the MoM impedance matrix $[Z]$ are achieved.

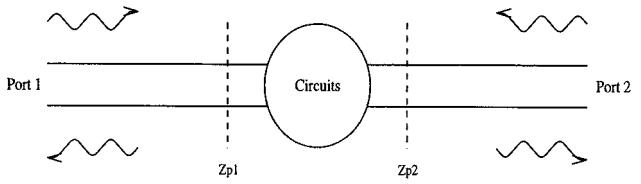

Fig. 6. Traveling-wave excitation.

IV. Traveling-Wave Excitation

The second class of excitation uses impressed current generators. It has been shown [20] that when the same set of basis functions are used, the impressed current excitation is equivalent to the voltage gap generator. An interesting impressed current model involves the use of traveling waves on both ports and far from the circuits. The remaining portion of the circuit can be expanded in subsectional basis functions. This mixed representation of the currents is an attempt to numerically simulate the matched connection between the input/output lines and the coaxial cables. In [13] and [19], the sinusoids are truncated after several cycles. It has been reported that the solutions are insensitive for lengths greater than three or four wavelengths [19] or five wavelengths [13]. The advantage of truncating the traveling waves is to avoid the singularities in the spectral domain that result from its infinite extent. On the other hand, as the length of the truncation is increased, the Fourier transform of the traveling wave tries to describe an equivalent delta function and a singular behavior using highly oscillatory functions, which is numerically inefficient and nonconverging [24]. When semiinfinite traveling waves are used [5], [24], the contributions due to the singularities and delta functions are evaluated analytically. The procedure shown below is a variation of those above, with modifications on both the traveling-wave basis functions and the corresponding extra weighting functions, which guarantees the convergence.

Consider an arbitrary circuit, as shown in Fig. 6, where the input and output lines extend to infinity. As we move away from the circuit, the current distribution on the lines resemble those of the respective infinite transmission lines. For example, if the circuit is excited from the port 1, the current on both ports far from the circuit can be approximated by

$$J_{z1} = f_{t1}(x)\left[e^{-j\beta_1(z-z_{p1})} - s_{11}e^{j\beta_1(z-z_{p1})}\right], \qquad z < z_{p1} \tag{29}$$

$$J_{z2} = s_{21}f_{t2}(x)e^{-j\beta_2(z-z_{p2})}, \qquad z > z_{p2} \tag{30}$$

where $f_{t1}(x)(f_{t2}(x))$ is a piecewise constant approximation of the transverse variation of the dominant mode at port 1 (2) with propagation constant $\beta_1(\beta_2)$. These functions and β's are previously obtained by a two-dimensional analysis. The remaining portion of the circuit is expanded in rooftop basis functions. The traveling-wave functions in (29) and (30) are nonzero at z_{p1} and z_{p2}, respectively, generating infinite charge distributions at these points. To assure the continuity of the currents, a ramp function $(R(z))$ is added to the end of the traveling-wave basis functions, resulting in

$$J_{z1}^{\text{inc}} = f_{t1}(x)e^{-j\beta_1(z-z_{p1})}[U(z_{p1}-z) + R(z-z_{p1}] \tag{31}$$

$$J_{z1}^{sca} = f_{t1}(x)e^{j\beta_1(z-z_{p1})}[U(z_{p1}-z) + R(z-z_{p1})] \tag{32}$$

$$J_{z2}^{sca} = f_{t2}(x)e^{-j\beta_2(z-z_{p2})}[U(z-z_{p2}) + R(z_{p2}-z)] \tag{33}$$

where $U(z)$ is the step function and the ramp function is given by

$$R(z) = \begin{cases} 1 - \dfrac{z}{\Delta z}, & 0 < z < \Delta z \\ 0, & \text{elsewhere} \end{cases} \tag{34}$$

and Δz is the discretization length of the adjacent rooftop section of the circuit. The current at ports 1 and 2 are now given by

$$J_{z1} = J_{z1}^{\text{inc}}(x, z) - s_{11}J_{z1}^{sca}(x, z) \tag{35}$$

$$J_{z2} = s_{21}J_{z2}^{sca}(x, z). \tag{36}$$

Furthermore, this accelerates the convergence of the integrals as the sine transform of the pure traveling waves in (29) and (30) decay with k_z^{-1}, while with the addition of the ramp functions, (35) and (36) decay with k_z^{-2}. This solution differs from those in [5], [13], and [19], where the problem was overcome by extending only the real part of the traveling wave for an extra quarter-wavelength, and truncating the sinusoids after an integer number of half-wavelengths [13], [19]. The boundary condition at the conducting surface of the circuit, after expanding the currents in traveling waves and rooftop functions, is given by

$$-s_{11}E_t(J_{z1}^{sca}) + s_{21}E_t(J_{z2}^{sca}) + \sum_{m_s=1}^{M_x} a_{xm_s}E_t(J_{xm_s}) + \sum_{m_s=1}^{M_z} a_{zm_s}E_t(J_{zm_s}) = -E_t(J_{z1}^{\text{inc}}) \tag{37}$$

where J_{xm_s} and J_{zm_s} are the rooftop basis functions. The conditions above are tested with a set of weighting functions that include all rooftop basis functions plus two extra functions (W_{zti}, $i = 1, 2$) centered at the interfaces between the traveling-wave sections and rooftop sections (z_{p1} and z_{p2}). The extra weighting functions, which are shown in Fig. 7, have a triangular z-dependency given by

$$g_{t1}(z) = \begin{cases} (z - z_{p1} + l_{w1})/l_{w1}, & (z_{p1} - l_{w1}) \le z \le z_{p1} \\ (z_{p1} + \Delta z_1 - z)/\Delta z_1, & z_{p1} \le z \le (z_{p1} + \Delta z_1) \\ 0 \quad \text{elsewhere} \end{cases} \tag{38}$$

$$g_{t2}(z) = \begin{cases} (z - z_{p2} + \Delta z_2)/\Delta z_2, & (z_{p2} - \Delta z_2) \le z \le z_{p2} \\ (z_{p2} + l_{w2} - z)/l_{w2}, & z_{p2} \le z \le (z_{p2} + l_{w2}) \\ 0, \quad \text{elsewhere} \end{cases} \tag{39}$$

and the same x-dependency as the traveling waves $f_{ti}(x)$. $\Delta z_1(\Delta z_2)$ is the discretization length of the rooftop section adjacent to port 1 (2), and $l_{w1}(l_{w2})$ is the length of the traveling-wave section at port 1 (2) where the boundary conditions are imposed. If the transmission line at port i extends from

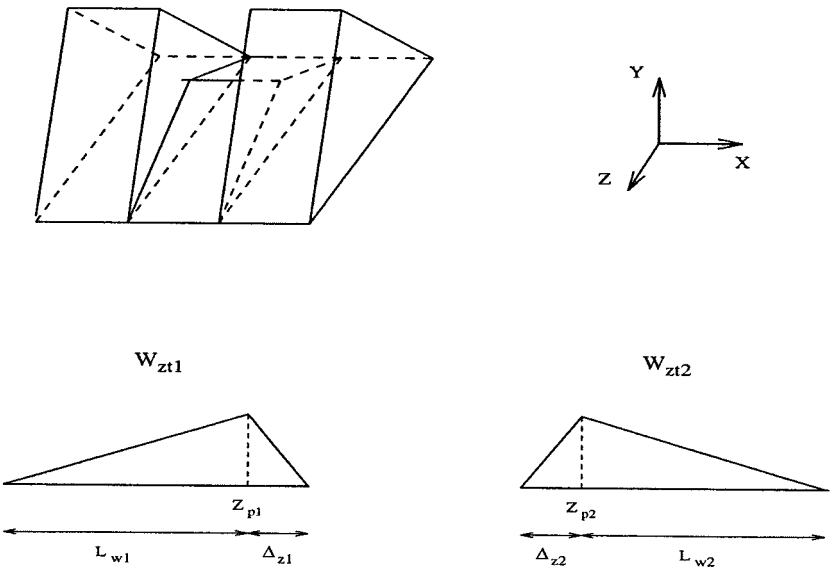

Fig. 7. Extra weighting functions.

x_{0ti} to x_{2ti} and we use M_{ti} basis functions in the transverse direction, then $f_{ti}(x)$ can be written as

$$f_{ti}(x) = \sum_{q=1}^{M_{ti}} c_{qi}[U\left(x - x_{(q-1)i}\right) - U(x - x_{qi})] \tag{40}$$

where c_{qi}'s are the coefficients of the current distribution across the stripline obtained from the two-dimensional analysis and $x_{qi} = x_{0ti} + q((x_{2ti} - x_{0ti})/M_{ti})\ q = 0, 1, \ldots, M_{ti}$. W_{zti} can be seen as a combination of rooftop functions weighted by the coefficients c_{qi}'s

$$W_{zti}(x, z) = f_{ti}(x)g_{zti}(z) = \sum_{q=1}^{M_{ti}} c_{qi}W_{zqi}(x, z), \qquad i = 1, 2 \tag{41}$$

where $W_{zqi}(x, z) = [U(x - x_{q-1}) - U(x - x_q)]g_{zti}(z)$. The basic difference between these extra weighting functions and those previously used is that in [5], [13], and [19] it was assumed that the extra weighting functions were symmetric, i.e., $l_{wi} = \Delta z_i$, while in our case, they are not. Although it may look like a small modification, it does have very important consequences. In the symmetric case, the length of the extra weighting functions ($2\Delta z_i$) diminish as we increase the number of basis functions of the adjacent rooftop section. This leads to the situation where the boundary conditions are imposed over a diminishing portion of the traveling wave (Δz_i) as we increase the number of rooftop basis functions. In the limit, the boundary conditions are no longer imposed over the traveling-wave sections. In our case, the traveling-wave sections are always being tested over a length l_{wi}, despite the number of basis functions used in the adjacent rooftop portion. It was observed that l_{wi} should be bigger than one-tenth of the wavelength of the quasi-TEM mode at the given port. In the symmetric case, that would require the use of less than ten basis functions per wavelength in the longitudinal direction, which is not enough to ensure convergence. When l_w is smaller than one-tenth of the wavelength, the S-parameters of the circuit are very sensitive to the value of l_w adopted. In our simulations, we have used values of l_w of at least a quarter-wavelength. This will be illustrated later in an example. After testing the boundary condition (37) with the set of weighting functions, the resulting equations are arranged in a matrix form $[Z][I] = [V]$

$$\begin{bmatrix} Z_{w1t1} & Z_{w1t2} & Z_{w1x} & Z_{w1z} \\ Z_{w2t1} & Z_{w2t2} & Z_{w2x} & Z_{w2z} \\ Z_{xt1} & Z_{xt2} & Z_{xx} & Z_{xz} \\ Z_{zt1} & Z_{zt2} & Z_{zx} & Z_{zz} \end{bmatrix} \begin{bmatrix} -s_{11} \\ s_{21} \\ a_x \\ a_z \end{bmatrix} = \begin{bmatrix} V_{w1t1} \\ V_{w2t1} \\ V_{xt1} \\ V_{zt1} \end{bmatrix}. \tag{42}$$

The submatrices Z_{xx}, Z_{xz}, Z_{zz}, and Z_{zx} represent the reaction between two rooftop functions, as in the case of a voltage gap generator. By reciprocity, these four submatrices form a symmetric portion of matrix $[Z]$. In the row matrices, Z_{wix} and Z_{wiz}, $i = 1, 2$, the fields due to rooftop basis functions are tested by the extra weighting functions W_{zti}. As these functions are combination of rooftop functions (41), the elements of Z_{wix} and Z_{wiz} are obtained similarly for Z_{zx} and Z_{zz}, respectively. Z_{xti} and Z_{zti} are column matrices where the fields due to the scattered traveling wave in port i are tested by rooftop weighting functions in x- and z-directions, respectively,

$$Z_{xtim_f} = \langle W_{xm_f}, E_x(J_{zi}^{sca})\rangle \tag{43}$$

$$= \frac{a}{4\pi}\sum_{n=1}^{\infty}\int_{-\infty}^{\infty}\left(\frac{\alpha_n}{jw\epsilon_2}\frac{\partial\tilde{G}_{A0z}^{s}}{\partial y} - jk_z\tilde{G}_{F0z}^{c}\right) \cdot \tilde{J}_{zi}^{sca}(\alpha_n, k_z)\tilde{W}_{xm_f}^{c}(\alpha_n, -k_z)\,dk_z \tag{44}$$

$$Z_{ztim_f} = \langle W_{zm_f}, E_z(J_{zi}^{sca})\rangle \tag{45}$$

$$= \frac{a}{4\pi}\sum_{n=1}^{\infty}\int_{-\infty}^{\infty}\left(\frac{-k_z}{w\epsilon_2}\frac{\partial\tilde{G}_{A0z}^{s}}{\partial y} + \alpha_n\tilde{G}_{F0z}^{c}\right) \cdot \tilde{J}_{zi}^{sca}(\alpha_n, k_z)\tilde{W}_{zm_f}^{s}(\alpha_n, -k_z)\,dk_z \tag{46}$$

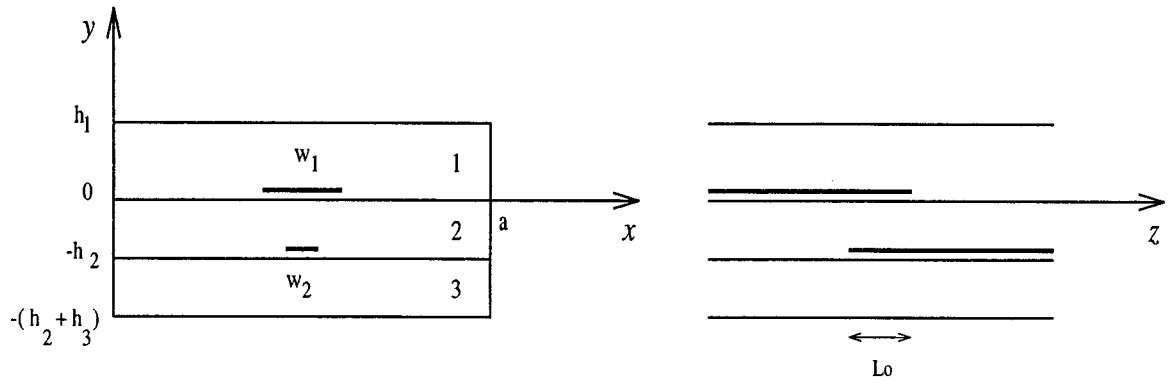

Fig. 8. Stripline coupling.

where $\tilde{J}_{z1}^{sca}$ and $\tilde{J}_{z2}^{sca}$ are the sine transforms of J_{z1}^{sca} of (32) and J_{z2}^{sca} of (33) and are given by

$$\tilde{J}_{z1}^{sca}(\alpha_n, k_z) = F_{t1}(\alpha_n)e^{jk_z z_{p1}} \cdot \left[\pi\delta(k_z+\beta_1)+\frac{1-e^{j(k_z+\beta_1)\Delta z_1}}{\Delta z_1(k_z+\beta_1)^2}\right] \quad (47)$$

$$\tilde{J}_{z2}^{sca}(\alpha_n, k_z) = F_{t2}(\alpha_n)e^{jk_z z_{p2}} \cdot \left[\pi\delta(k_z-\beta_2)+\frac{1-e^{-j(k_z-\beta_2)\Delta z_2}}{\Delta z_2(k_z-\beta_2)^2}\right] \quad (48)$$

$$F_{ti}(\alpha_n) = \frac{2}{a\alpha_n}\sum_{q=1}^{M_{ti}} c_{qi}\left[\cos\left(\alpha_n x_{(q-1)i}\right)-\cos(\alpha_n x_{qi})\right]. \quad (49)$$

In Z_{witj}, $i = 1, 2$, the fields due to the scattered traveling wave in port j are tested by the weighting functions W_{zti}. From (41), these elements are obtained similarly to Z_{zti} (46). The elements of the independent vector $[V]$ of (42) are given by

$$V_{xt1m_f} = -\langle W_{xm_f}, E_x(J_{z1}^{\text{inc}})\rangle \quad (50)$$

$$= -\frac{a}{4\pi}\sum_{n=1}^{\infty}\int_{-\infty}^{\infty}\left(\frac{\alpha_n}{jw\epsilon_2}\frac{\partial\tilde{G}_{A0z}^{s}}{\partial y}-jk_z\tilde{G}_{F0z}^{c}\right) \cdot \tilde{J}_{z1}^{\text{inc}}(\alpha_n, k_z)\tilde{W}_{xm_f}^{c}(\alpha_n, -k_z)\,dk_z \quad (51)$$

$$V_{zt1m_f} = -\langle W_{zm_f}, E_z(J_{z1}^{\text{inc}})\rangle \quad (52)$$

$$= -\frac{a}{4\pi}\sum_{n=1}^{\infty}\int_{-\infty}^{\infty}\left(\frac{-k_z}{w\epsilon_2}\frac{\partial\tilde{G}_{A0z}^{s}}{\partial y}+\alpha_n\tilde{G}_{F0z}^{c}\right) \cdot \tilde{J}_{z1}^{\text{inc}}(\alpha_n, k_z)\tilde{W}_{zm_f}^{s}(\alpha_n, -k_z)\,dk_z \quad (53)$$

where $\tilde{J}_{z1}^{\text{inc}}$ is the sine transforms of J_{z1}^{inc} (31), and is given by

$$\tilde{J}_{z1}^{\text{inc}}(\alpha_n, k_z) = F_{t1}(\alpha_n)e^{jk_z z_{p1}} \cdot \left[\pi\delta(k_z-\beta_1)+\frac{1-e^{j(k_z-\beta_1)\Delta z_1}}{\Delta z_1(k_z-\beta_1)^2}\right]. \quad (54)$$

Similar to matrix $[Z]$, the two first rows of $[V]$ are obtained as a combination of elements of the form V_{zt1}. Once all the elements of the linear system (42) are known, the coefficients of the scattered traveling waves at ports 1 and 2 are obtained directly from the numerical solution of the given system. When the circuit is excited from port 2, the current distribution far from it can be approximated by

$$J_{z1} = s_{12}J_{z1}^{sca}(x, z) \quad (55)$$

$$J_{z2} = J_{z2}^{\text{inc}}(x, z) - s_{22}J_{z2}^{sca}(x, z) \quad (56)$$

where J_{z1}^{sca} and J_{z2}^{sca} are given, respectively, by (32) and (33), and J_{z2}^{inc} is equal to

$$J_{z2}^{\text{inc}} = f_{t2}(x)e^{j\beta_2(z-z_{p2})}[U(z-z_{p2})+R(z_{p2}-z)]. \quad (57)$$

After expanding the remaining portion of the circuit in rooftop basis functions and imposing the boundary conditions, we obtain a linear system given by

$$\begin{bmatrix} Z_{w1t1} & Z_{w1t2} & Z_{w1x} & Z_{w1z} \\ Z_{w2t1} & Z_{w2t2} & Z_{w2x} & Z_{w2z} \\ Z_{xt1} & Z_{xt2} & Z_{xx} & Z_{xz} \\ Z_{zt1} & Z_{zt2} & Z_{zx} & Z_{zz} \end{bmatrix}\begin{bmatrix} s_{12} \\ -s_{22} \\ a_x \\ a_z \end{bmatrix} = \begin{bmatrix} V_{w1t2} \\ V_{w2t2} \\ V_{xt2} \\ V_{zt2} \end{bmatrix}. \quad (58)$$

The $[Z]$ matrix is the same as for the excitation from port 1, and the elements of the independent vector $[V]$ are obtained similarly to the previous case with $\tilde{J}_{z1}^{\text{inc}}$ substituted by the sine transform of J_{z2}^{inc} (57)

$$\tilde{J}_{z2}^{\text{inc}}(\alpha_n, k_z) = F_{t2}(\alpha_n)e^{jk_z z_{p2}} \cdot \left[\pi\delta(k_z+\beta_2)+\frac{1-e^{-j(k_z+\beta_2)\Delta z_2}}{\Delta z_2(k_z+\beta_2)^2}\right]. \quad (59)$$

The elements of the auxiliary matrix s are obtained directly from the solution of the linear systems (42) and (58). The S-parameters are obtained from the elements of matrix s as

$$S_{11} = \frac{b_1}{a_1}_{|a_2=0} = \frac{-I_1^{\text{ref}}\sqrt{Z_{o1}}}{+I_1^{\text{inc}}\sqrt{Z_{o1}}}_{|I_2^{\text{inc}}=0} = s_{11} \quad (60)$$

$$S_{21} = \frac{b_2}{a_1}_{|a_2=0} = \frac{+I_2^{\text{ref}}\sqrt{Z_{o2}}}{+I_1^{\text{inc}}\sqrt{Z_{o1}}}_{|I_2^{\text{inc}}=0} = \sqrt{\frac{Z_{o2}}{Z_{o1}}}\,s_{21} \quad (61)$$

$$S_{12} = \frac{b_1}{a_2}_{|a_1=0} = \frac{-I_1^{\text{ref}}\sqrt{Z_{o1}}}{-I_2^{\text{inc}}\sqrt{Z_{o2}}}_{|I_1^{\text{inc}}=0} = \sqrt{\frac{Z_{o1}}{Z_{o2}}}\,s_{12} \quad (62)$$

$$S_{22} = \frac{b_2}{a_2}_{|a_1=0} = \frac{+I_2^{\text{ref}}\sqrt{Z_{o2}}}{-I_2^{\text{inc}}\sqrt{Z_{o2}}}_{|I_1^{\text{inc}}=0} = s_{22}. \quad (63)$$

As we know that $S_{12} = S_{21}$ for reciprocal networks, then from (61) and (62)

$$S_{12} = S_{21} = \sqrt{s_{12}s_{21}}. \quad (64)$$

A. Numerical Evaluation of the Impedance Matrix Z

The elements of the linear systems (42) and (58) basically involve two kinds of reactions. The first is between two rooftop

functions, which has already been described. In the second, the fields produced by a traveling-wave basis functions are tested by a rooftop basis function. There are three sources of numerical instabilities when evaluating these elements: the poles of the Green's functions, the oscillatory and slow decaying behavior of the integrand, and the singularities of the traveling-wave basis functions in spectral domain. The first two are common to the reaction of two rooftop functions, and are solved following the same procedure. The singularities of the traveling waves are treated analytically, as illustrated for the case of Z_{zt1}. The singularities of the sine transform of J_{z1}^{sca} of (47) include a delta function and a first order pole at $k_z = -\beta_1$. It can be shown that the contribution of the delta function is equal to $j\pi R_\beta$, where R_β is the residue of the integrand at $k_z = -\beta_1$. The remaining part should be integrated in the principal value sense. Removing the pole from the integrand

$$Z_{zt1m_f} = \frac{a}{4\pi}\sum_{n=1}^{\infty}\left\{ j\pi R_\beta + \left(\int_{-\infty}^{-k_{z2}} + \int_{-k_{z1}}^{\infty}\right)\mathrm{Int}_{zt1}\,dk_z + \int_{-k_{z2}}^{-k_{z1}}\left(\mathrm{Int}_{zt1} - \frac{R_\beta}{k_z+\beta_1}\right)dk_z + P.V.\int_{-k_{z2}}^{-k_{z1}}\frac{R_\beta}{k_z+\beta_1}\,dk_z\right\} \quad (65)$$

where

$$\mathrm{Int}_{zt1} = \left(\frac{-k_z}{w\epsilon_2}\frac{\partial \tilde{G}_{A0z}^{s}}{\partial y} + \alpha_n \tilde{G}_{F0z}^{c}\right) \cdot \tilde{J}_{z1p}^{sca}(\alpha_n, k_z)\tilde{W}_{zm_f}^{s}(\alpha_n, -k_z) \quad (66)$$

$$\tilde{J}_{z1p}^{sca}(\alpha_n, k_z) = F_{t1}(\alpha_n)e^{jk_z z_{p1}}\frac{1-e^{j(k_z+\beta_1)\Delta z_1}}{\Delta z_1(k_z+\beta_1)^2}. \quad (67)$$

As an alternative procedure we can use $\tilde{J}_{z1p}^{sca}$ of (67) as the sine transform of the reflected traveling wave at port 1 (J_{z1}^{sca}) and distort the integration path with a semicircle of infinitesimal radius around the pole $k_z = -\beta_1$, in the third quadrant. This would be similar to the approach used for the poles of the Green's functions, and both approaches yield the same result.

V. Numerical Examples

As an example, consider a stripline coupling shown in Fig. 8. The waveguide with dimensions $a = 10$ mm, and $b = 7.62$ mm is filled with two dielectric layers of the same thickness $h_2 = h_3 = 0.635$ mm, and dielectric constants $\epsilon_{r2} = 10.2$ and $\epsilon_{r3} = 2.2$. A stripline of width $w_1 = 1.9$ mm at the $y = 0$ interface is coupled with another of width $w_2 = 1$ mm at the $y = -h_2$ interface. The stripline overlap is 1.5 mm. When using a voltage gap generator, the striplines were truncated 32 mm from the end, and for traveling-wave excitation, the rooftop section extended for 8 mm from the end of the striplines. The convergence of the magnitude of the reflection coefficient at port 1 (S_{11}) with the number of longitudinal basis functions is shown in Fig. 9. Only one transverse basis function was used. For the voltage gap generator, the convergence is reached with about 15 basis functions per wavelength of the dominant mode (λ_g), while the traveling-wave generator required about 25 basis per wavelength, for the same accuracy.

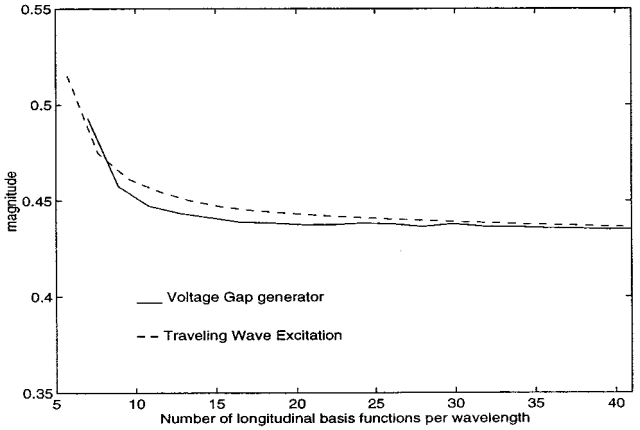

Fig. 9. Convergence of the magnitude of S_{11} with the number of longitudinal basis functions per wavelength.

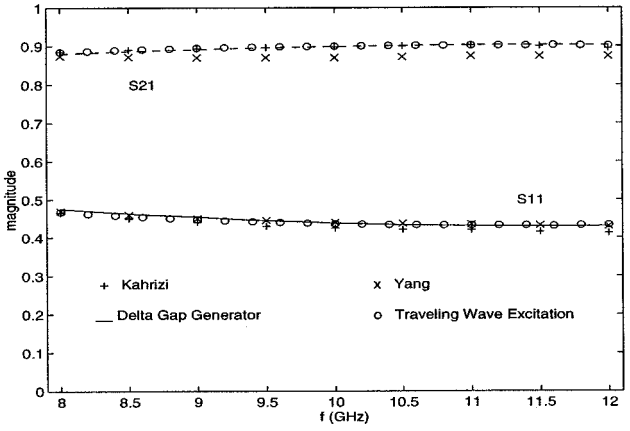

Fig. 10. Magnitude of S-parameters for a microstrip coupling. $a = 10$ mm, $b = 7.62$ mm, $h_1 = 6.35$ mm, $h_2 = h_3 = 0.635$ mm, $\epsilon_{r1} = 1$, $\epsilon_{r2} = 10.2$ and $\epsilon_{r3} = 2.2$, $w_1 = 1.9$ mm, $w_2 = 1$ mm, and $l = 1.5$ mm.

Fig. 10 shows the amplitudes of the reflection and transmission coefficients as the frequency varies from 8–12 GHz, for both excitation methods. The results are compared with those of a parallel-plate waveguide with the same dielectric filling obtained by Kahrizi [10] using space-domain analysis, and with those for the case of infinite dielectric layers without top ground plane by Yang [5] using the spectral-domain analysis. Despite the differences of the structures, the S-parameters present very similar behavior, with a small discrepancy for the S_{21} of [5] due to radiation losses.

An interesting result is shown in Fig. 11. The magnitude of S_{11} is shown as we vary the length l_w of the extra weighting functions. This corresponds to the distance where the boundary conditions are imposed on the traveling-wave section. From Fig. 11, we observe two very distinct regions. One is for l_w smaller than one-tenth of the wavelength, where the magnitude of S_{11} varies rapidly, and worsens for smaller values of l_w. For l_w greater than one-tenth of the wavelength, the reflection coefficient has a smooth variation. We have adopted the value l_w equal to a quarter-wavelength as a convergence value, although any value of l_w in this second region will provide results within the expected numerical error. In this case, we have used

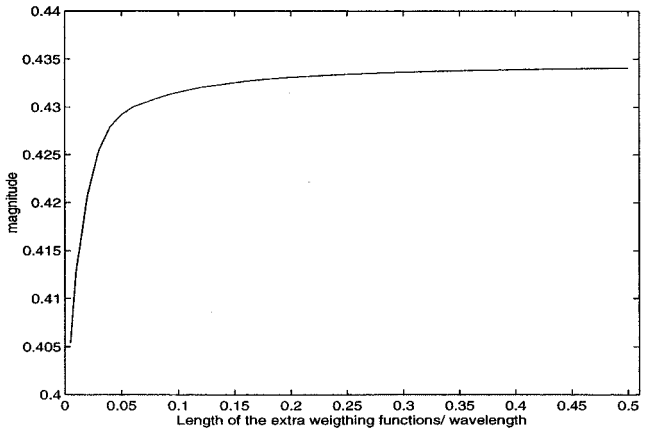

Fig. 11. Convergence of the magnitude of S_{11} with the length l_w of the extra weighting functions per wavelength.

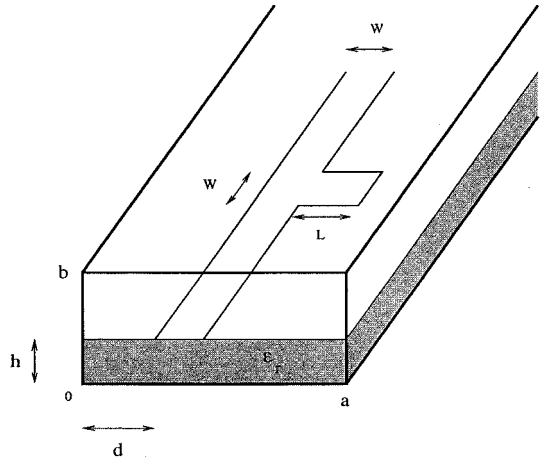

Fig. 12. Microstrip stub.

30 basis longitudinal basis functions on the rooftop section, which corresponds to a discretization length Δz equal to 0.017 wavelengths. If we had used symmetrical extra weighting functions, it would have led to an error of approximately 5%.

Consider now the microstrip stub shown in Fig. 12. The waveguide of dimensions $a = 10$ mm and $b = 7.62$ mm is filled with a dielectric layer of constant $\epsilon_r = 10.65$ and thickness $h = 1.27$ mm. The transmission line has width $w = 1.40$ mm and is placed at a distance $d = 3.6$ mm from the closest vertical wall. The stub has the same width as the line, and length $L = 2.16$ mm. Figs. 13 and 14 show, respectively, the magnitude and phase of the transmission coefficient as the frequency varies from 7.5–12 GHz. Also shown are measurements and theoretical results obtained by Jackson [2] for the unshielded microstrip case. It is observed that the results closely matches the quasi-static prediction of a phase jump of 180° near the resonance. This happens because at this frequency range, the quasi-TEM dominant mode is the only one that propagates in the structure. The open microstrip [2] case, on the other hand, shows a reduced peak phase due to radiation or conductor losses (measurement). A similar effect is also observed in Fig. 13 for the magnitude of the transmission coefficient.

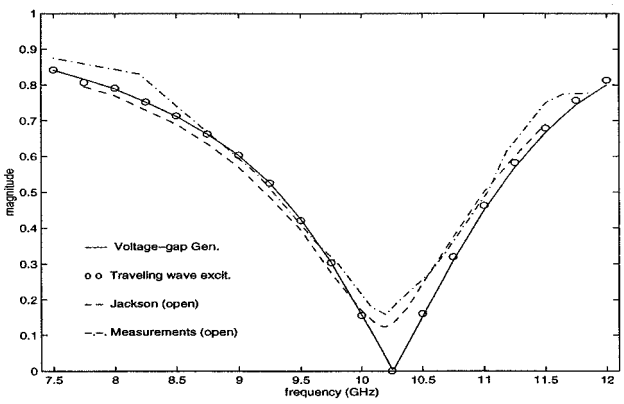

Fig. 13. Magnitude of S_{21} for the microstrip stub. $a = 10$ mm, $b = 10.62$ mm, $h = 1.27$ mm, $e_r = 10.65$, $w = 1.40$ mm, and $L = 2.16$ mm.

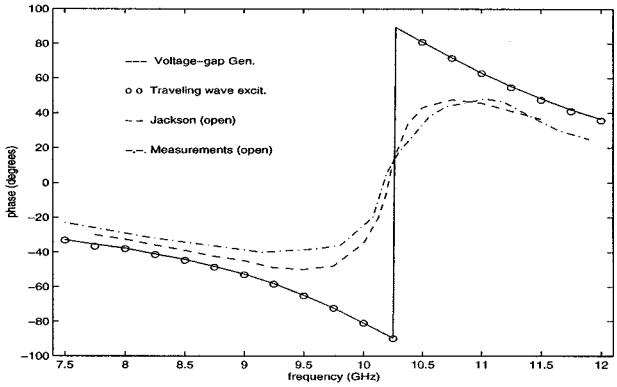

Fig. 14. Phase of S_{21} for the microstrip stub. $a = 10$ mm, $b = 10.62$ mm, $h = 1.27$ mm, $e_r = 10.65$, $w = 1.40$ mm, and $L = 2.16$ mm.

As a last example, consider the a microstrip gap with an overlay half-wave resonator, as shown in Fig. 15. The waveguide has dimensions $a = b = 20$ mm, and is filled with two dielectric layers of the same dielectric constant $\epsilon_r = 2.33$ and thickness $h = 0.8382$ mm. The transmission line has width $w = 2.3$ mm, with a gap of $g = 1.0$ mm. The parasitic resonator is placed symmetrically over the gap, with the same width of the transmission line, and length $L = 27.3$ mm. The magnitude of the reflection and transmission coefficients are shown in Fig. 16, together with numerical results and measurements obtained by Yeung [9] for the case of an open multilayered structure. It is observed that the resonance frequency shifts slightly toward 4 GHz.

VI. Comments on Voltage Gap Generator and Traveling-Wave Excitation

One problem of the voltage gap generator is the condition number of the impedance matrix $[Z]$ of MoM close to resonances. It is a consequence of the finite extent of the circuit resulting from the truncation. These points should be carefully avoided to ensure the accuracy of the results. Our simulations have shown that the condition number increases quickly as we approach one of the resonant frequencies, but the system is ill conditioned only within a very close proximity of those points. When using traveling-wave excitation, this problem is not present, due to the infinite extent of the circuit. Another

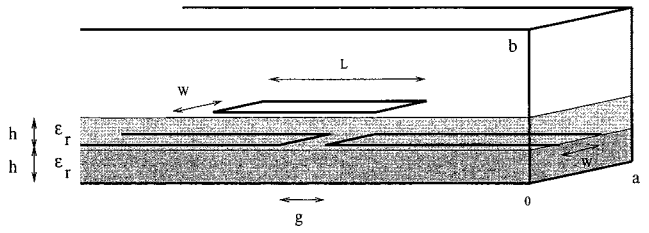

Fig. 15. Microstrip gap with overlay half-wave resonator.

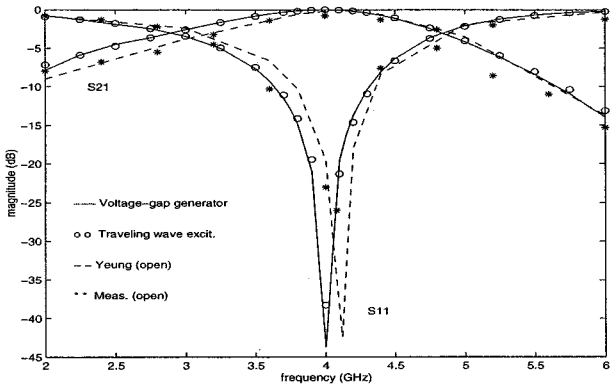

Fig. 16. Magnitude of S_{11} and S_{21} for the microstrip gap with overlay resonator. $a = b = 20$ mm, $h = 0.8382$ mm, $e_r = 2.33$, $w = 2.3$ mm, $g = 1.0$ mm, and $L = 27.3$ mm.

advantage of the traveling waves is the control we have on the incident wave on the circuit. For structures where the dominant quasi-TEM is the only one that propagates, it really does not make a difference, as all higher order modes are evanescent. However, when more than one mode propagates at a given physical port, the traveling-wave excitation provides a way of separating the contributions due to each of them. The traveling-wave excitation usually requires a small rooftop section between the traveling wave and circuits. Typically, a half-wavelength-long rooftop section is sufficient for getting stable solutions. This results in a smaller MoM linear system than for the case of voltage gap excitation, where sections of one to two wavelengths are required. Although the system is smaller, the computational time spent for the traveling-wave excitation was found to be bigger than when using a voltage gap generator. In fact, around 2.5 times longer for the same density of basis functions. This is a consequence of extensive use of symmetry in the impedance matrix $[Z]$ when using voltage gap generator. Two elements of $[Z]$ are equal when the basis and weighting functions corresponding to one are shifted versions in z-direction of the functions corresponding to the other. For the traveling-wave excitation, the same happens in the rooftop submatrices (Z_{xx}, Z_{xz}, Z_{zx}, and Z_{zz}). However, no such redundancies are present for the reaction between the traveling-wave basis functions and the rooftop testing functions, and all the elements of the corresponding submatrices have to be numerically evaluated. The S-parameters are either obtained directly from the solution of the linear system for the traveling-wave excitation, or by the use of the matrix pencil technique for the voltage gap generator. The apparent advantage of the traveling-wave excitation diminishes as the matrix pencil is a very quick and reliable procedure. As observed from the numerical examples, the results from both excitation techniques are very close and the same accuracy is obtained.

VII. Conclusions

This paper has presented a full-wave analysis of MICs in multilayer dielectric media in a rectangular waveguide. It shows a procedure that permits an accurate and faster numerical evaluation of the moment matrix, without the limitations of previous FFT routines. Both voltage gap generator and traveling-wave excitation have been used and compared. The use of asymmetrical weighting functions has been introduced in the latter, and its importance for achieving convergence was discussed.

References

[1] T. Itoh, *Numerical Techniques for Microwave and Millimeter-Wave Passive Structures*. New York: Wiley, 1989.

[2] R. W. Jackson, "Full-wave finite-element analysis of irregular microstrip discontinuities," *IEEE Trans. Microwave Theory Tech.*, vol. 37, pp. 81–89, Jan. 1989.

[3] M. Horno and F. Medina, "Multilayer planar structures for high directivity directional coupler design," *IEEE Microwave Theory Tech.*, vol. MTT-34, pp. 1442–1449, Dec. 1986.

[4] N. K. Das and D. M. Pozar, "A generalized spectral-domain Green's function for multilayer dielectric substrates with application to multilayer transmission lines," *IEEE Trans. Microwave Theory Tech.*, vol. MTT-35, pp. 326–335, Mar. 1987.

[5] H. Yang and N. G. Alexopoulos, "Basic blocks for high-frequency interconnects: Theory and experiment," *IEEE Trans. Microwave Theory Tech.*, vol. 36, pp. 1258–1264, Aug. 1988.

[6] W. P. Harokopus Jr. and P. B. Katehi, "Characterization of microstrip discontinuities on multilayer dielectric substrates including radiation losses," *IEEE Trans. Microwave Theory Tech.*, vol. 37, pp. 2058–2066, Dec. 1989.

[7] J. Basterrechea and M. F. Catedra, "Computation of microstrip S-parameters using a CG–FFT scheme," *IEEE Trans. Microwave Theory Tech.*, vol. 42, pp. 234–240, Feb. 1994.

[8] W. Schwab and W. Menzel, "On the design of planar microwave components using multilayer structures," *IEEE Trans. Microwave Theory Tech.*, vol. 40, pp. 67–71, Jan. 1992.

[9] E. K. L. Yeung, J. C. Beal, and Y. M. M. Antar, "Multilayer microstrip structure analysis with matched load simulation," *IEEE Trans. Microwave Theory Tech.*, vol. 43, pp. 143–149, Jan. 1995.

[10] M. Kahrizi, "A three-dimensional space domain approach for the analysis of printed circuit problems," Ph.D. dissertation, Dept. Elect. Eng., Syracuse Univ., Syracuse, NY, 1992.

[11] Y. L. Chow, J. J. Yang, D. G. Fang, and G. E. Howard, "A closed-form spatial Green's function for the thick microstrip substrate," *IEEE Trans. Microwave Theory Tech.*, vol. 39, pp. 588–592, Mar. 1991.

[12] H. Yang, A. Nakatani, and J. A. Castaneda, "Efficient evaluation of spectral integrals in the moment method solution of microstrip antennas and circuits," *IEEE Trans. Antennas Propagat.*, vol. 38, pp. 1127–1130, July 1990.

[13] U. V. Gothelf and A. Ostergaard, "Full-wave analysis of a two slot microstrip filter using a new algorithm for computation of the spectral integrals," *IEEE Trans. Microwave Theory Tech.*, vol. 41, pp. 101–108, Jan. 1993.

[14] J. C. Rautio and R. F. Harrington, "An electromagnetic time-harmonic analysis of shielded microstrip circuits," *IEEE Trans. Microwave Theory Tech.*, vol. MTT-35, pp. 726–730, Aug. 1987.

[15] A. Hill and V. K. Tripathi, "An efficient algorithm for the three-dimensional analysis of passive microstrip components and discontinuities for microwave and millimeter-wave integrated circuits," *IEEE Trans. Microwave Theory Tech.*, vol. 39, pp. 83–91, Jan. 1991.

[16] C. J. Railton and S. A. Meade, "Fast rigorous analysis of shielded planar filters," *IEEE Trans. Microwave Theory Tech.*, vol. 40, pp. 978–985, May 1992.

[17] S. Hashemi-Yeganeh, "On the summation of double infinite series field computations inside rectangular cavities," *IEEE Trans. Microwave Theory Tech.*, vol. 43, pp. 641–646, Mar. 1995.

[18] G. V. Eleftheriades, J. R. Mosig, and M. Guglielmi, "A fast integral equation technique for shielded planar circuits defined on nonuniform meshes," *IEEE Trans. Microwave Theory Tech.*, vol. 44, pp. 2293–2296, Dec. 1996.
[19] R. W. Jackson and D. M. Pozar, "Full-wave analysis of microstrip open-end and gap discontinuities," *IEEE Trans. Microwave Theory Tech.*, vol. MTT-33, pp. 1036–1042, Oct. 1985.
[20] G. V. Eleftheriades and J. R. Mosig, "On the network characterization of planar passive circuits using the method of moments," *IEEE Trans. Microwave Theory Tech.*, vol. 44, pp. 438–445, Mar. 1996.
[21] P. B. Katehi and N. G. Alexopoulos, "Frequency-dependent characteristics of microstrip discontinuities in millimeter-wave integrated circuits," *IEEE Trans. Microwave Theory Tech.*, vol. MTT-33, pp. 1029–1035, Oct. 1985.
[22] Y. Hua, "On techniques for estimating parameters of exponentially damped/undamped sinusoids in noise," Ph.D. dissertation, Dept. Elect. Eng., Syracuse Univ., Syracuse, NY, 1988.
[23] T. K. Sarkar and O. M. Pereira, "Using the matrix pencil method to estimate the parameters of a sum of complex exponentials," *IEEE Antennas Propagat. Mag.*, vol. 37, pp. 48–55, Feb. 1995.
[24] N. K. Das and D. M. Pozar, "Multiport scattering analysis of general multilayered printed antennas fed by multiple feed ports: Part I—Theory," *IEEE Trans. Antennas Propagat.*, vol. 40, pp. 469–481, May 1992.

Odilon M. C. Pereira Filho (S'94–M'97) received the B.S.E.E. degree from the Federal University of Pernambuco (UFPE), Brazil, in 1987, the M.S.E.E. degree from the Pontifical Catholic University of Rio de Janeiro, Rio de Janeiro, Brazil, in 1991, and the Ph.D. degree from Syracuse University, Syracuse, NY, in 1997.

He was a Research Engineer at EMBRATEL—Brazilian Company of Telecommunications from 1988 to 1989, a Research Associate at the UFPE from March to August 1992, and a Research Engineer at IBM, Hopewell Junction, NY, from 1997 to 1998. From August to December 1998 he was an Adjunct Professor at the University of Pernambuco, and since then he has been a Visiting Professor. His main interest is in numerical electromagnetics with applications in microwaves and antennas.

Tapan K. Sarkar (S'69–M'76–SM'81–F'92) received the B.Tech. degree from the Indian Institute of Technology, Kharagpur, India, in 1969, the M.Sc.E. degree from the University of New Brunswick, Fredericton, NB, Canada, in 1971, and the M.S. and Ph.D. degrees from Syracuse University; Syracuse, NY, in 1975.

From 1975 to 1976, he was with the TACO Division, General Instruments Corporation. He was with the Rochester Institute of Technology, Rochester, NY, from 1976 to 1985. He was a Research Fellow at the Gordon McKay Laboratory, Harvard University, Cambridge, MA, from 1977 to 1978. He is currently a Professor in the Department of Electrical and Computer Engineering, Syracuse University. His current research interests deal with numerical solutions of operator equations arising in electromagnetics and signal processing with application to system design. He has authored or co-authored over 210 journal articles and numerous conference papers, has written chapters in 28 books, and has authored over ten books, including *Iterative and Self Adaptive Finite-Elements in Electromagnetic Modeling*, (Norwood, MA: Artech House, 1998). He is on the editorial board of the *Journal of Electromagnetic Waves and Applications*.

Dr. Sarkar is a member of Sigma Xi and International Union of Radio Science Commissions A and B. He is a Registered Professional Engineer in the State of New York. He received the 1979 Best Paper Award of the IEEE TRANSACTIONS ON ELECTROMAGNETIC COMPATIBILITY and the 1997 Best Paper Award presented at the National Radar Conference. He received the 1996 College Engineering Research Award and the Chancellor's Citation for Excellence in Research in 1998 presented by Syracuse University. He was an associate editor for the *IEEE Antennas and Propagation Society Newsletter*, and the Technical Program Chairman for the 1988 IEEE Antennas and Propagation Society International Symposium and URSI Radio Science Meeting. He has been appointed U.S. Research Council Representative to many URSI General Assemblies. He was the chairman of the Intercommission Working Group of International URSI on Time Domain Metrology (1990–1996). He received one of the "best solution" awards in May 1977 presented at the Rome Air Development Center (RADC) Spectral Estimation Workshop. He received the title of Docteur Honoris Causa from Universite Blaise Pascal, Clermont Ferrand, France, in 1998.